Proceedings of the ASME 2010 3rd Joint US-European Fluids Engineering Summer Meeting and 8th International Conference on Nanochannels, Microchannels, and Minichannels
FEDSM-ICNMM2010
August 1-5, 2010, Montreal, Canada

FEDSM-ICNMM2010-30482

SIMULATION OF HYPERSONIC VISCOUS FLOW PAST A 2D CIRCULAR CYLINDER USING LATTICE BOLTZMANN METHOD

R. Kamali
Shiraz University
Shiraz, Fars, IRAN

A.H. Tabatabaee Frad
Shiraz University
Shiraz, Fars, IRAN

ABSTRACT

It is known that the Lattice Boltzmann Method is not very effective when it is being used for the high speed compressible viscous flows; especially complex fluid flows around bodies. Different reasons have been reported for this unsuccessfulness; Lacking in required isotropy in the employed lattices and the restriction of having low Mach number in Taylor expansion of the Maxwell Boltzmann distribution as the equilibrium distribution function, might be mentioned as the most important ones. In present study, a new numerical method based on Li et al. scheme is introduced which enables the Lattice BoltzmannMethod to stably simulate the complex flows around a 2D circular cylinder. Furthermore, more stable implementation of boundary conditions in Lattice Boltzmann method is discussed.

INTRODUCTION

The Lattice Boltzmann Method (LBM) has been attracting a large amount of attention since its introduction by McNamara and Zanetti in 1988 [1]. Gradually it has become an alternative method for simulating fluid flows and because of its kinetic origins it has wider range of applicability than conventional descriptions since LBM also works in mesoscopic scales. Having an algorithm which is capable of parallel processing also helps LBM be one of the hottest topics in computational fluid dynamics in the past decade. Although LBM has been very successful in simulation of isothermal and incompressible flows there has been little success in simulating compressible thermal flows. Different reasons have been reported for the unsuccessfulness; Lacking in required isotropy in the employed lattices and the restriction of having low Mach number in Taylor expansion of Maxwell Boltzmann distribution as the equilibrium distribution function, might be mentioned as the most important ones. The remedy for the former is to use multispeed models. Presented model by Watari and Tsutahara [2,3] is the prime example for this and according to Chen et al. [4,5] could be used to construct a higher order Lattice Boltzmann model (Watari and Tsutahara used Hermite expansion of Maxwell Boltzmann distribution and keeps up to forth order of flow velocity). But the problem of multispeed models is the limited range of stability of the energy and velocity. The latter is also investigated and the substitution of the Maxwell Boltzmann distribution for other functions which satisfy the same constraints as every equilibrium distribution function must do has been proposed. Kataoka and Tsutahara [6] and Qu et al. [7] presented brand new distribution functions in their models which were able to recover compressible Euler equations; Kataoka and Tsutahara [8] also presented a model which is capable of recovering compressible Navier Stokes equations. Most of these models are restricted to low speed and low temperature flows. The above presented models have been extended to high Mach numbers and high temperatures by the introduction of modified numerical schemes. Studies [7, 9-12] have shown that in order to be able to well capture discontinuities there must be enough artificial dissipation in numerical schemes which seems to be needed more than the amount comes from the collision term of the BGK lattice Boltzmann method. Either one must use TVD, WENO or ENO schemes or the required dissipation must be added directly to the numerical scheme of the model. Qu et al. used a TVD scheme that makes their model is able to capture discontinuities in inviscid high speed compressible flows. While using Watari and Tsutahara's lattice and equilibrium distribution function, Gan et al. [13] employed a modified Lax-Wendroff scheme plus artificial viscosity instead of second order upwind scheme used by original authors and succeeded in modeling fluid flows with high Mach numbers containing strong shocks and discontinuities. Pan et al. [14] utilized a first order upwind scheme with artificial viscosity along with Kataoka and Tsutahara's discrete velocity model and simulated successfully high speed compressible flows with discontinuities. Recently Li et al. [12] introduced a new model encompassing strong features of previous models: It is a multispeed model and employs an extension of Qu et al. equilibrium distribution

function for Navier Stokes equations and uses a shock capturing TVD and WENO scheme for solving the differential form of the lattice Boltzmann equation. Although this model is successful in modeling high speed compressible viscous flows like Couette flow, Riemann problems and shock reflections, in simulation of a complex flow around a circular cylinder for Mach numbers higher than Mach=3.0 it fails. Other than that, the model is also impotent in very low pressures and for example comparing Li et al. results with Kim's data, which we adopted for validation of our results, is not possible because the stream's pressure is around 486pa [15].

In the present study, a new model is introduced which exhibits the LBM ability to work out the complexity of the 2D external flow in hypersonic compressible viscous flow. A hypersonic viscous compressible flow of Mach number of $\boldsymbol{M = 6.0}$ *past a cylinder at a very low pressure has been tested. Simulations conducted stably and with a acceptable amount of error. Trend of the results clearly demonstrates LB-BGK's lacking in enough dissipation for handling oscillations in high speed compressible flows.*

NOMENCLATURE

$\boldsymbol{c}_i$ *discrete particle velocity in i direction*
$\tilde{c}$ *characteristic velocity*
D *dimension*
E *total energy*
f_i *density distribution function*
f_i^{eq} *density equilibrium distribution function*
h_i *total energy distribution function*
h_i^{eq} *total energy equilibrium distribution function*
Pr *Prandtl number*
p *pressure*
R *gas constant*
ρ *density*
T_c *characteristic temperature*
T *temperature*
τ_h, τ_h *energy and density relaxation times*
$\boldsymbol{u}$ *macroscopic velocity*

COUPLED DOUBLE DISTRIBUTION FUNCTION LBM BY LI ET AL.

The double distribution function method, with a distribution function for density and another for energy, was used for compressible LBM by Li et al. They employed Guo's double distribution function model [16] in which the usual internal energy distribution function is replaced by the total energy distribution function. The evolution equations for density and total energy are as follows respectively

$$\frac{\partial f_i}{\partial t} + (\boldsymbol{c}_i \cdot \boldsymbol{\nabla}) f_i = -\frac{1}{\tau_f}(f_i - f_i^{eq}) \qquad i = 1,2,\dots,N \tag{1}$$

$$\frac{\partial h_i}{\partial t} + (\boldsymbol{c}_i \cdot \boldsymbol{\nabla}) h_i = -\frac{1}{\tau_h}(h_i - h_i^{eq}) + \frac{1}{\tau_{hf}}(\boldsymbol{c}_i \cdot \boldsymbol{u})(f_i - f_i^{eq}) \qquad i = 1,2,\dots,N \tag{2}$$

Where f_i *is the density distribution function and* h_i *is the total energy distribution function,* f_i^{eq} *and* h_i^{eq} *are the corresponding equilibrium distribution functions,* $\boldsymbol{c}_i$ *is the discrete particle velocity in* i *direction,* $\boldsymbol{u}$ *is the macroscopic velocity,* τ_h *and* τ_f *are energy and density relaxation times and* τ_{hf} *is defined as*

$$\frac{1}{\tau_{hf}} = \frac{1}{\tau_h} - \frac{1}{\tau_f} \tag{3}$$

The relation between two relaxation times, τ_h *and* τ_f*, is given by* Pr*:*

$$Pr = \frac{\tau_f}{\tau_h} \tag{4}$$

Therefore one can set the Prandtl number by adjusting τ_h *and* τ_f*. Macroscopic variables computing from density distribution function are defined as follows:*

$$\rho = \sum_{i=1}^{N} f_i \tag{5}$$

$$\rho u_\alpha = \sum_{i=1}^{N} f_i c_{i\alpha} \tag{6}$$

A D2Q12 lattice which ensures isotropy up to sixth rank lattice tensor is used

$$\boldsymbol{c}_i = \begin{cases} \tilde{c}\left\{cos\left[\frac{(i+1)\pi}{2}\right], sin\left[\frac{(i+1)\pi}{2}\right]\right\} & i = 1,3,4,5 \\ \sqrt{2}\tilde{c}\left\{cos\left[\frac{(2i-1)\pi}{4}\right], sin\left[\frac{(2i-1)\pi}{4}\right]\right\} & i = 5,6,7,8 \\ 2\tilde{c}\left\{cos\left[\frac{(i-9)\pi}{2}\right], sin\left[\frac{(i-9)\pi}{2}\right]\right\} & i = 9,10,11,12 \end{cases} \tag{7}$$

Where $\tilde{c}$ *is the characteristic velocity and* $\tilde{c} = \sqrt{RT_c}$ *in which* T_c *is the characteristic temperature. This characteristic temperature is set to around maximum stagnation temperature in the problem.*

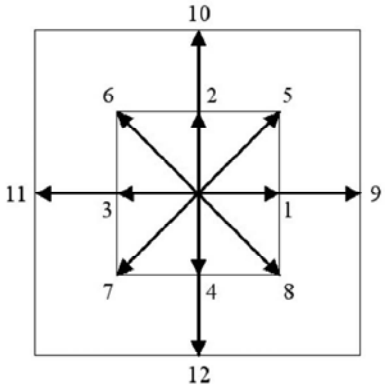

Fig. 1. *The D2Q12 Square Lattice used by Li et al.*

Li et al. introduced two different kinds of equilibrium distribution function in their work; one is based on the Maxwell Boltzmann distribution and the other on Qu et al. work [7]. The latter is for high speed flows and the former is for moderate and low speed flows. In this study since we focused on high speed flows around 2D circular cylinder we leave off the one for low speed flows. Any function who wants to play the role of the equilibrium distribution function in the evolution equation for density distribution function Eq. (1) must satisfy the following constraints

$$\rho = \sum_{i=1}^{N} f_i^{eq} \tag{8.a}$$

$$\rho u_\alpha = \sum_{i=1}^{N} f_i^{eq} c_{i\alpha} \tag{8.b}$$

$$p\delta_{\alpha\beta} + \rho u_\alpha u_\beta = \sum_{i=1}^{N} f_i^{eq}\, c_{i\alpha} c_{i\beta} \tag{8.c}$$

$$p\left(u_\alpha \delta_{\beta\gamma} + u_\beta \delta_{\gamma\alpha} + u_\gamma \delta_{\alpha\beta}\right) + \rho u_\alpha u_\beta u_\gamma = \sum_{i=1}^{N} f_i^{eq} c_{i\alpha} c_{i\beta} c_{i\gamma} \tag{8.d}$$

$$\rho u^2 + Dp = \sum_{i=1}^{N} f_i^{eq} c_i^2 \tag{8.f}$$

$$[\rho u^2 + (D+2)p]u_\alpha = \sum_{i=1}^{N} f_i^{eq} c_i^2 c_{i\alpha} \tag{8.g}$$

Li et al. calculated their new equilibrium distribution function according to the Qu et al. work. But lots of work they had to do since the previous model recovered compressible Euler equations and Prandtl number was equal to specific heat ratio. Finally, the new equilibrium distribution functions with the capability of recovering compressible Navier Stokes equations and without previous defects were introduced with $f_i^{eq} = \rho_i$ *where all are given Annex A.*

The same procedure as the density distribution function, was not taken for total energy distribution function and for the sake of simplicity, Li et al. devised the following relation

$$h_i^{eq} = [E + (\boldsymbol{c}_i - \boldsymbol{u})\cdot\boldsymbol{u}]f_i^{eq} + \varpi_i \frac{P}{\tilde{c}^2} RT \tag{9}$$

Which is capable of satisfying the following constraints required for the equilibrium total energy distribution functions

$$\sum_i h^{eq} = \rho E \tag{10.a}$$

$$\sum_i c_{i\alpha} h^{eq} = (\rho E + p)u_\alpha \tag{10.b}$$

$$\sum_i c_{i\alpha} c_{i\beta} h^{eq} = (\rho E + 2p)u_\alpha u_\beta + p(E + RT)\,\delta_{\alpha\beta} \tag{10.c}$$

Where $E = bRT/2 + u^2/2$ *is the total energy.* ϖ_i *are constants which should be obtained by solving Eq. (10).*

One can calculate temperature by

$$T = \frac{2}{bR}\left[\frac{1}{\rho}\sum_i h^{eq} - \frac{u^2}{2}\right] \tag{11}$$

Therefore it would be very easy to couple the two distributions by using the thermal equation of state for computing pressure

$$p = p(\rho, T) \tag{12}$$

For solving Eq. (1, 2) Li et al. used a second order TVD scheme for spatial discretization and a second order Implicit-Explicit Runge-Kutta (IMEX) scheme for temporal discretization.

NEW FINITE DIFFERENCE SCHEME

The numerical method employed with Li et al. does not work at low pressure and/or high Mach number viscous flows around a 2D circular cylinder. In order to make the Lattice Boltzmann model applicable to these kinds of flows we introduced a new finite difference scheme to the model. As it mentioned in part I, either you have to use high resolution schemes or add required dissipation directly to the numerical scheme. Since the second order TVD scheme employed by Li et al. was not applicable and the fifth order WENO scheme [12] that we used didn't work either, we resort to test a finite difference scheme and add artificial dissipation.

In order to solve the hyperbolic Eqs. (1, 2), we take first order IMEX (Implicit Explicit) Runge-Kutta scheme [17] which includes implicit and explicit time discretizations for collision and other terms respectively; In the first step for density distribution function we will have:

$$f_i^{t+\frac{\Delta t}{2}} = \frac{f_i^t + \frac{\Delta t}{\tau_f} f_i^{eq}}{1 + \frac{\Delta t}{\tau_f}} \tag{13}$$

And then,

$$\frac{f_i^{t+\Delta t} - f_i^t}{\Delta t} = \frac{1}{\tau_f}\left(f_i^{eq} - f_i^{t+\frac{\Delta t}{2}}\right) - c_{i\xi}\nabla_\xi f_i^{t+\frac{\Delta t}{2}} \tag{14}$$

For the calculation of the last terms in the right hand side of the above Eq. (14), as it mentioned, Li et al. adopt a second order TVD scheme to discretize (spatial discretization). In order to have a successful simulation, we employ upwind schemes and an artificial viscosity as follows:

$$\theta_I = l \times MAX\left(\frac{|P_{I+1} - 2P_I + P_{I-1}|}{|P_{I+1} + 2P_I + P_{I-1}|}, \frac{|P_{I+2} - 2P_{I+1} + P_I|}{|P_{I+2} + 2P_{I+1} + P_I|}\right)$$

$$\Gamma_\xi = u_\xi \frac{\Delta t}{\Delta r_\xi}$$

$$F_{Artificial-Viscosity} = \theta_I |\Gamma_\xi|\left(1 - |\Gamma_\xi|\right)\frac{\Delta r_\xi^2}{2\Delta t}\frac{\partial^2 f_i}{\partial r_\xi^2}$$

$$H_{Artificial-Viscosity} = \theta_I |\Gamma_\xi|\left(1 - |\Gamma_\xi|\right)\frac{\Delta r_\xi^2}{2\Delta t}\frac{\partial^2 h_i}{\partial r_\xi^2}$$

l is a constant for determining the amount artificial viscosity. In the calculation of $\frac{\partial^2 f_i}{\partial r_\xi^2}$ *and* $\frac{\partial^2 h_i}{\partial r_\xi^2}$ *one could use a second order central difference scheme. The above artificial*

viscosity term is, with a slight modification, very similar to Gan et al. work [13] which is based on Jameson's viscosity term [18, 19]. $F_{Artificial-Viscosity}$ is directly added to the Eq. (14) and the final forms of the equation is:

$$\frac{f_i^{t+\Delta t} - f_i^t}{\Delta t} = \frac{1}{\tau_f}\left(f_i^{eq} - f_i^{t+\frac{\Delta t}{2}}\right) - c_{i\xi}\nabla_\xi f_i^{t+\frac{\Delta t}{2}} + F_{Artificial-Viscosity} \quad (16)$$

The same procedure is taken for total energy distribution function h_i.

MORE STABLE BOUNDARY CONDITION IMPLEMENTATION

For satisfying the wall boundary condition, Li et al. employed Guo method (non-equilibrium extrapolation boundary condition) [20] which has been proposed for low Mach number incompressible fluid flows. There seems to be no more accurate boundary condition method for compressible high Mach number flows and they might as well used it since it has attracted lots of attention [12, 21] in recent years. In Guo's non-equilibrium extrapolation boundary condition method the distribution functions are decomposed into two parts: equilibrium and non-equilibrium parts

$$f_i = f_i^{eq} + f_i^{non-eq} \quad (17)$$

Therefore, the distribution function on the wall is decomposed into two parts. Usually velocity and temperature are known on the wall and for computing the equilibrium distribution function, one more unknown, which Guo considered to be density, needs to be extrapolated from the adjacent node. The non-equilibrium part,

$$f_i^{non-eq} = f_i - f_i^{eq} \quad (18)$$

is also assumed to be equal the one of the nearest fluid node. But our study showed extrapolating the density makes the simulations very unstable and pressure extrapolation is much more stable than that. As a result, it is recommended, especially in high speed compressible flows, this point be taken into account when satisfying boundary conditions.

NUMERICAL SIMULATIONS AND RESULTS

Couette Flow

To exhibit the rightness of the discussion in part IV, we first present the result of the simulation of Couette flow at a Mach number of $M = 12.0$. In this simulation a second order upwind scheme is employed but in implementing Guo's method we extrapolate pressure instead of density. It should be mentioned that the simulation without doing this is so unstable and quickly diverges.

In our Couette flow simulation the upper wall is apart from the lower by a distance of H and it starts to move with at speed U while both walls are at temperature T_0. The exact solution along the vertical axis y is

$$T = T_0 + \frac{Pr}{2c_p}U^2\frac{y}{H}\left(1 - \frac{y}{H}\right) \quad (19)$$

disregarding the accuracy of the simulations, this can show clearly that our modification of extrapolating pressure instead of density has a great effect on the stability of the simulations.

High Speed Flow around a Circular Cylinder

In order for us to be able to compare our results with experiment, we used Kim's results and its conditions for the simulations.

In the physical domain, a cylinder is at the origin of the $x-y$ plane. A square of $[0,1]\times[0,1]$ in $\xi-\eta$ plane is the computational domain. The mapping relationship between the two domains is

$$x = -\left[R_x - (R_x - R)\frac{1}{a}tanh(\tilde{c}\xi)\right]cos(\theta\eta) \quad (20)$$

$$y = +\left[R_y - (R_y - R)\frac{1}{a}tanh(\tilde{c}\xi)\right]sin(\theta\eta) \quad (21)$$

Where R is the cylinder radius and R_x and R_y are outer radii of the physical domain in x and y directions respectively. $\tilde{c}$ is the parameter used for the adjustment of arrangement and distribution of the grid nodes. $\theta = \frac{\pi}{2}$, $R_x = 5R$ and $R_y = 10R$ are set in our simulations. A mesh of 150×50 is generated in $\xi-\eta$ plane and $\tilde{c} = 2.9$. A sketch of physical mesh is shown in Fig. 3. The flow conditions are $Re_\infty = 2.5\times10^5$, $M_\infty = 6.0$, $T_\infty = 280K$, $p_\infty = 486pa$ and the wall temperature is $T_w = 300K$. Specific heat ratio $\gamma = 1.4$ and the Prandtl number is set to 0.72. The cylinder radius is $0.005m$.

The following boundary conditions are employed in the simulations. Free stream conditions are used as the outer boundary condition; so the distribution function values are set identical to the values of the equilibrium distributions obtained from the initial values. Zeroth order extrapolation of distribution functions is used at the exit and it means all the macroscopic variables are attained from the upstream. On the wall, no-slip isothermal conditions are used. The no-slip wall boundary condition is applied considering the point made in the previous part.

Spatial Discretization

As it mentioned in part II upwind schemes are employed for spatial discretization. Fifth, third and first order accurate upwind schemes were used respectively in order to achieve better accuracy and stability.

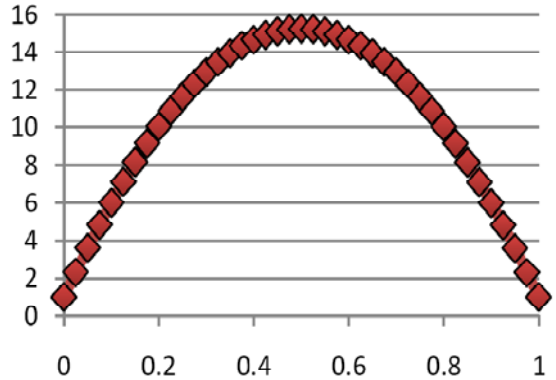

Fig. 2. *Couette flow: Temperature profile*

Fifth Order Upwind Scheme

The last term in Eq. (14) is discretized using fifth order upwind scheme as follows:

$$c_{i\xi}\nabla_{\xi}f_i = c_{i\xi}\frac{\begin{matrix}-2f_{i,I-3}+15f_{i,I-2}-60f_{i,I-1}\\+20f_{i,I}+30f_{i,I+1}-3f_{i,I+2}\end{matrix}}{60\Delta\xi}, \quad c_{i\xi}\geq 0 \qquad (22.a)$$

$$c_{i\xi}\nabla_{\xi}f_i = c_{i\xi}\frac{\begin{matrix}+3f_{i,I-2}-30f_{i,I-1}-20f_{i,I}\\+60f_{i,I+1}-15f_{i,I+2}+2f_{i,I+3}\end{matrix}}{60\Delta\xi}, \quad c_{i\xi}< 0 \qquad (22.b)$$

For satisfying the wall boundary condition we used Guo's extrapolation boundary condition method. For near the wall grid nodes, we substitute fifth order upwind Eq. (23) with third and first order upwind schemes respectively.

The Mach and Pressure contours are shown in Fig. 4. And Fig. 5. There is an considerable amount of error in the prediction of the shock stand-off distance in front of the cylinder.

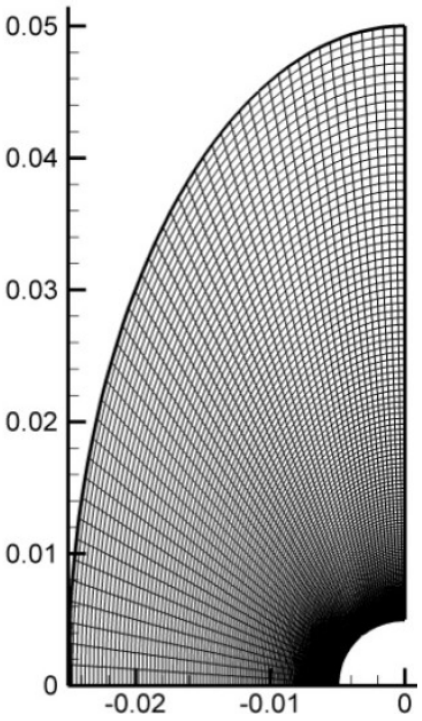

Fig. 3. *Physical Mesh used in the Simulations*

Employing a lower order scheme might as well be tested to see if it decreases the error and improves the accuracy.

Third Order Upwind Scheme

Employing a third order upwind scheme discretizing the convective term in Eq. (14) we have:

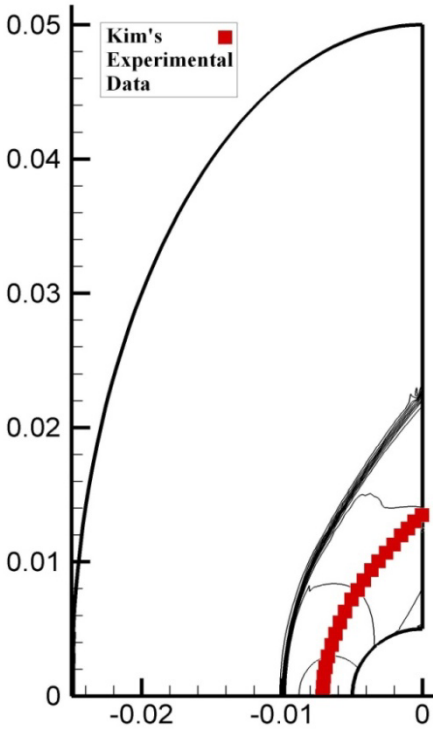

Fig. 4. *Flow Past a Cylinder (5th Order): Mach Contours*

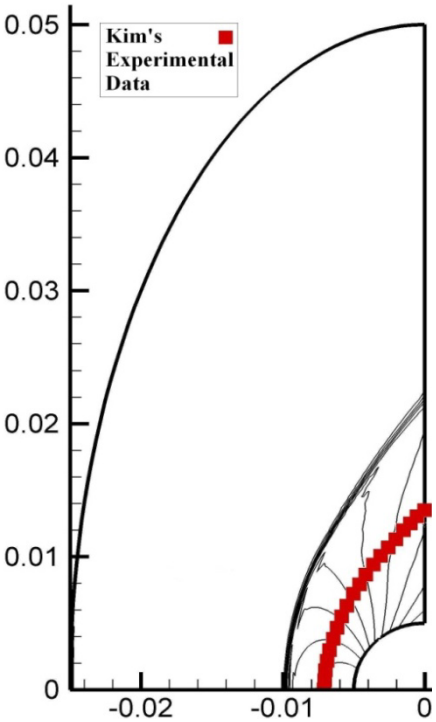

Fig. 5. *Flow Past a Cylinder (5th Order): Pressure Contours*

$$c_{i\xi}\nabla_\xi f_i = c_{i\xi}\frac{+f_{i,I-2} - 6f_{i,I-1} + 3f_{i,I} + 2f_{i,I+1}}{6\Delta\xi}, \quad c_{i\xi} \geq 0 \qquad (23.a)$$

$$c_{i\xi}\nabla_\xi f_i = c_{i\xi}\frac{-2f_{i,I-1} - 3f_{i,I} + 6f_{i,I+1} - f_{i,I+2}}{6\Delta\xi}, \quad c_{i\xi} < 0 \qquad (23.b)$$

Again Mach and Pressure contours are shown in Fig. 6. There is still a large amount of error in the prediction of the shock stand-off distance in front of the cylinder. Surprisingly, error has been decreased and employing third order upwind scheme instead of fifth order seemingly produces better results. Considering the trend of the computations, employing even lower order schemes seems likely to produce more accurate results.

First Order Upwind Scheme

In order to see if lowering the order of spatial discretization improves the result, for the third simulation, first order upwind scheme is employed to discretize the convective term in Eq. (14) and we have:

$$c_{i\xi}\nabla_\xi f_i = c_{i\xi}\frac{f_{i,I} - f_{i,I-1}}{\Delta\xi}, c_{i\xi} \geq 0 \qquad (24.a)$$

$$c_{i\xi}\nabla_\xi f_i = c_{i\xi}\frac{f_{i,I+1} - f_{i,I}}{\Delta\xi}, c_{i\xi} < 0 \qquad (24.b)$$

Mach and Pressure contours are shown in Fig. 7. The error in the prediction of the shock stand-off distance in front of the cylinder has been decreased again. It is seen clearly that results becomes more accurate as the order of spatial discretization decreases.

DISCUSSIONS

In this study, it is shown that simulation of a complex hypersonic flow past a cylinder using Lattice Boltzmann method can be done stably and accurately. The reason why powerful numerical schemes with high performance like TVD and WENO do not work with Finite Difference Lattice Boltzmann Methods (FDLBM) seems very questionable. On the other hand, there are finite difference lattice Boltzmann models that by adding the suitable amount of dissipation were able to work beyond the expected limits [13, 14]. The problem seems to be closely related to the BGK collision term which is unable to produce enough dissipation to handle the oscillations along with high resolution schemes. Therefore it seems that employing a collision term which has more similar behavior to the original Boltzmann collision integral could result in more successful simulations with high resolution schemes and in the future studies in compressible high speed viscous flows must be considered.

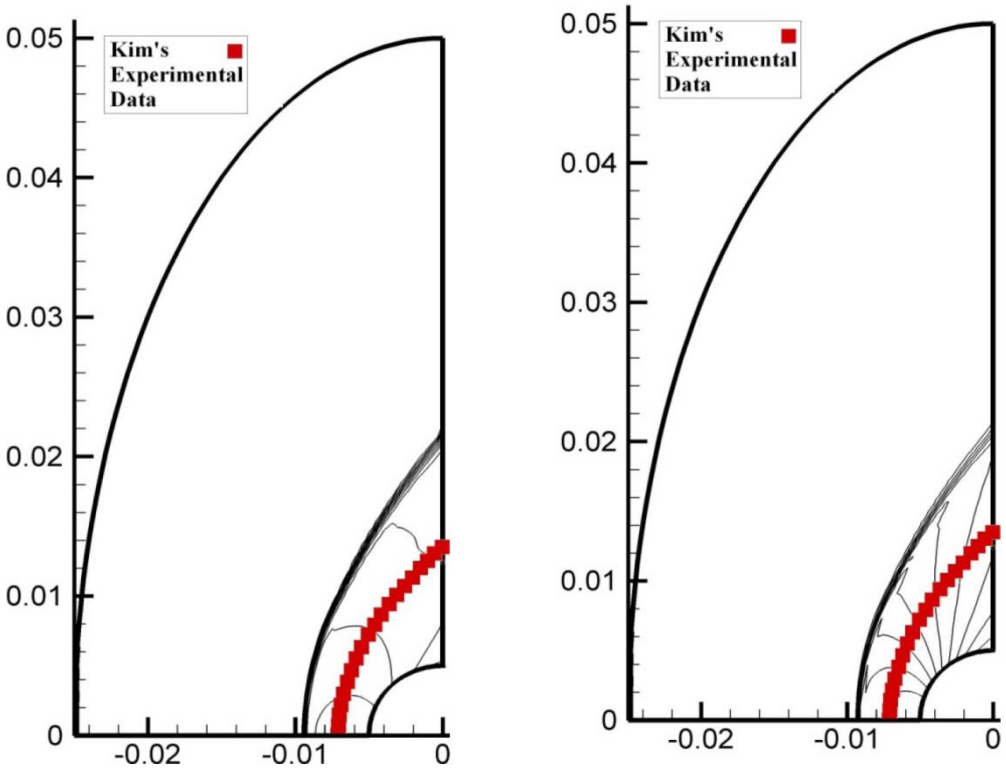

(a) *(b)*

Fig. 6. *Flow Past a Cylinder (3rd Order Upwind Scheme): (a) Mach Contours; (b) Pressure Contours*

Nevertheless, there is a startling anomaly in our results. We expect to have more accurate results with higher order spatial discretizations; however, the computations effect the exact opposite. The reason why still remains unknown to us.

In the three simulations we conducted with different order of spatial discretization the same value of $l = 50$ *was used as the dissipation term's factor. For considering the amount of artificial dissipation effect on the accuracy of the simulations we pick our most accurate results came from first order upwind schemes and reduce* l *form* 50 *to* 15*. Below in Fig. 7 results from the simulation with* $l = 15$ *and* $l = 50$ *are shown. The accuracy has considerably been improved.*

ACKNOWLEDGMENTS

We want to thank dear Qing Li for his helpful discussions.

REFERENCES

[1] G. R. McNamara, and G. Zanetti, Use of the Boltzmann Equation to Simulate Lattice-Gas Automata Phys. Rev. Lett. 61, 2332–2335

[2] M. Watari, and M. Tsutahara, Two-dimensional thermal model of the finite-difference lattice Boltzmann method with high spatial isotropy, Phys. Rev. E 67 (2003) 036306.

[3] M. Watari, Finite difference lattice Boltzmann method with arbitrary specific heat ratio applicable to supersonic flow simulations, Physica A 382 502–522, 2007

[4] H. Chen, and X. Shan, Fundamental conditions for N-th-order accurate lattice Boltzmann models, Physica D (2008) 2003.

[5] H. Chen, I. Goldhirsch, and S. A. Orszag, Discrete Rotational Symmetry, Moment Isotropy,and Higher Order Lattice Boltzmann Models, J. Sci. Comput. 34, 87–112, 2008

[6] T. Kataoka and M. Tsutahara, Lattice Boltzmann method for the compressible Euler equations, Phys. Rev. E 69, 056702 (2004).

[7] K. Qu, C. Shu, and Y. T. Chew, Alternative method to construct equilibrium distribution functions in lattice-Boltzmann method simulation of inviscid compressible flows at high Mach number, Rev. E ***75****, 036706 , (2007).*

[8] T. Kataoka and M. Tsutahara, Lattice Boltzmann model for the compressible Navier-Stokes equations with flexible specific-heat ratio, Phys. Rev. E 69, 035701(R) (2004).

[9] G. Yan, Y. Chen, and S. Hu, Simple Lattice Boltzmann Model for Simulating flows with shock wave, Phys. Rev. E ***59****, 454 (1999).*

[10] F. L. Hinton, M. N. Rosenbluth, S. K. Wong, Y. R. Lin-Liu, and R. L. Miller, Modified Lattice Boltzmann method for compressible fluid simulations, Phys. Rev. E ***63****, 061212 (2001).*

[11] W. Shi, W. Shyy, and R. Mei, Finite-Difference-Based Lattice Boltzmann Method for Inviscid Compressible Flows, Numer. Heat Transfer, Part B ***40****, 1 (2001).*

[12] Q. Li, Y. L. He, Y. Wang, and W. Q. Tao, Coupled double-distribution-function lattice Boltzmann method for the compressible Navier-Stokes equations, Phys. Rev. E ***76****, 056705, (2007).*

[13] Y. Gan, A. Xu, G. Zhangb, X. Yub, and Y. Li, Two-dimensional lattice Boltzmann model for compressible flows with high Mach number, Physica A 387 1721–1732, (2008).

[14] X. F. Pan, A. Xu, G. Zhang, and S. Jiang, Lattice Boltzmann Approach to High-Speed Compressible Flows, Int. J. Mod. Phys. C 18(11), 1747-1764 (2007).

[15] C. Kim, (1956). Experimental Studies of Supersonic Flow Past a Circular Cylinder, Journal of the Physics Society of Japan, Vol. 11(4).

[16] Z. Guo, C. Zheng, B. Shi, and T. S. Zhao, Thermal Lattice Boltzmann Equations for Low Mach number Flows: Decoupling Model, Phys. Rev. E ***75****, 036704 (1998).*

[17] Q. Li, Y.L. He, Y. Wang, and G.H. Tang, Three-dimensional non-free-parameter lattice-Boltzmann model and its application to inviscid compressible flows, Physica A 373 2101–2108, (2009).

[18] A. Jameson, Steady-State Solution of the Euler Equations for Transonic Flow, Adv. Sci. Comput. 37–69 (1982).

[19] A. Jameson, W. Schmidt, and E. Turkel, Numerical Solutions of the Euler Equations by Finite Volume Methods using Runge–Kutta Time-Stepping Schemes, AIAA Paper, pp. 81–1259 (1981) unpublished.

[20] Z. Guo, C. Zheng, and B. Shi, An Extrapolation Method for Boundary Condition in Lattice Boltzmann Method, Phys. Fluids 14, 2007 (2002).

[21] G. H. Tang, W. Q. Tao, and Y. L. He, Thermal Boundary Condition for the Thermal Lattice Boltzmann Equation, Phys. Rev. E ***72****, 016703 (2005).*

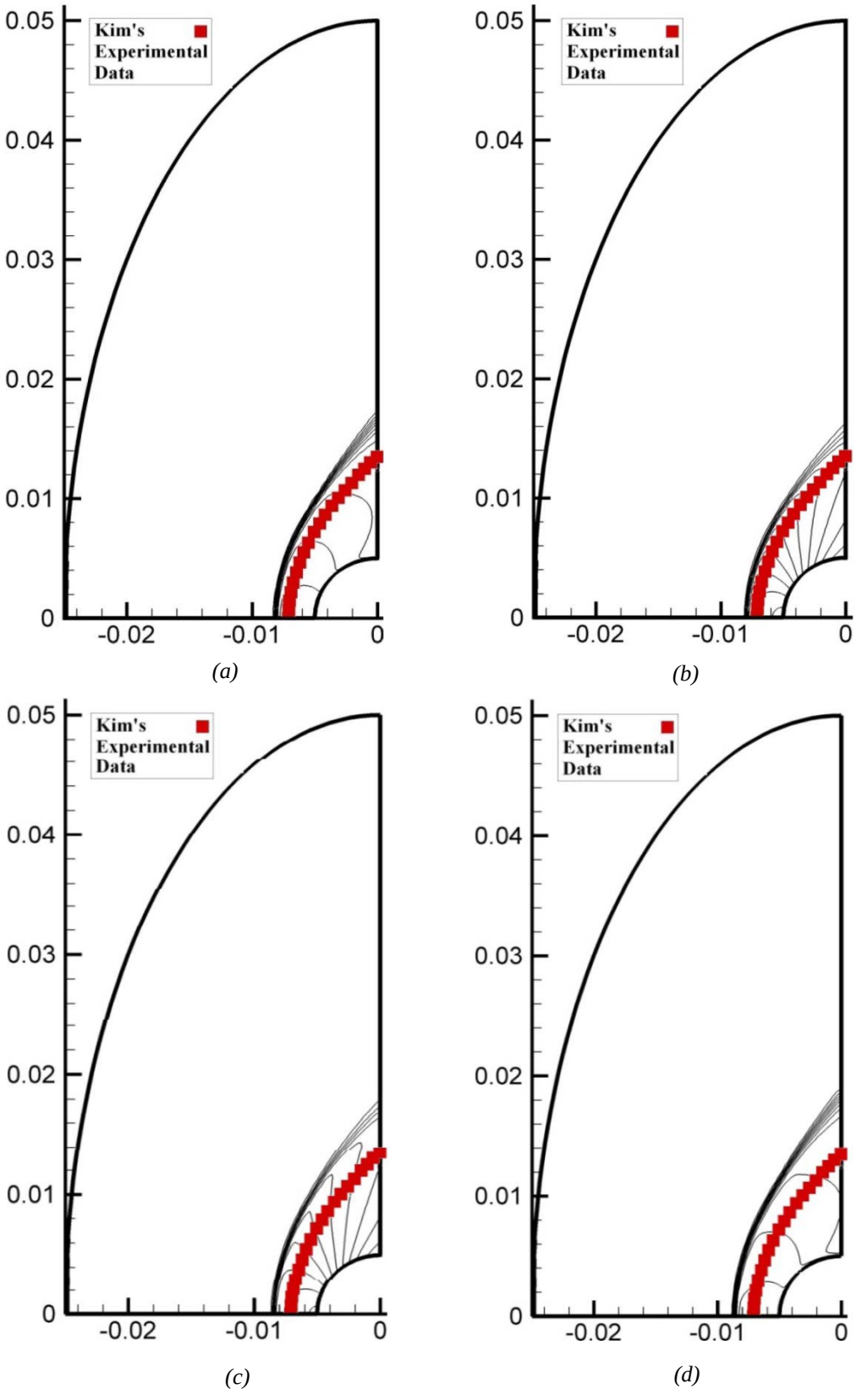

Fig. 7. *Flow Past a Cylinder (1st Order Upwind Scheme): (a) Mach Contours; (b) Pressure Contours (1st Order Upwind Scheme with $l = 15$): (c) Mach Contours; (d) Pressure Contours*

ANNEX A

$$\rho_0 = \frac{\rho}{4}[\bar{u}^4 + 5\bar{P}^2 - 10\bar{P} + 4 + 4\bar{u}^2\bar{v}^2 + \bar{v}^4 + (10\bar{P} - 5)(\bar{u}^2 + \bar{v}^2)] \quad (A.1)$$

$$\rho_1 = -\frac{\rho}{6}[-4\bar{u}^2 + 3\bar{P}^2 + \bar{u}^4 - 4\bar{P} + 3\bar{P}\bar{v}^2 + 3\bar{u}\bar{v}^2 + 9\bar{P}\bar{u}^2 + 6\bar{P}\bar{u} + 3\bar{u}^2\bar{v}^2 - 4\bar{u} + \bar{u}^3] \quad (A.2)$$

$$\rho_2 = -\frac{\rho}{6}[-4\bar{v}^2 + 3\bar{P}^2 + \bar{v}^4 - 4\bar{P} + 3\bar{P}\bar{u}^2 + 3\bar{v}\bar{u}^2 + 9\bar{P}\bar{v}^2 + 6\bar{P}\bar{v} + 3\bar{u}^2\bar{v}^2 - 4\bar{v} + \bar{v}^3] \quad (A.3)$$

$$\rho_3 = -\frac{\rho}{6}[-4\bar{u}^2 + 3\bar{P}^2 + \bar{u}^4 - 4\bar{P} + 3\bar{P}\bar{v}^2 - 3\bar{u}\bar{v}^2 + 9\bar{P}\bar{u}^2 - 6\bar{P}\bar{u} + 3\bar{u}^2\bar{v}^2 + 4\bar{u} - \bar{u}^3] \quad (A.4)$$

$$\rho_4 = -\frac{\rho}{6}[-4\bar{v}^2 + 3\bar{P}^2 + \bar{v}^4 - 4\bar{P} + 3\bar{P}\bar{u}^2 - 3\bar{v}\bar{u}^2 + 9\bar{P}\bar{v}^2 - 6\bar{P}\bar{v} + 3\bar{u}^2\bar{v}^2 + 4\bar{v} - \bar{v}^3] \quad (A.5)$$

$$\rho_5 = \frac{\rho}{4}[\bar{u}\bar{v}^2 + \bar{u}\bar{v} + \bar{P}\bar{u} + \bar{P}\bar{v} + \bar{v}\bar{u}^2 + 0.5\bar{P}^2 + \bar{u}^2\bar{v}^2 + \bar{P}\bar{u}^2 + \bar{P}\bar{v}^2] \quad (A.6)$$

$$\rho_6 = \frac{\rho}{4}[-\bar{u}\bar{v}^2 - \bar{u}\bar{v} - \bar{P}\bar{u} + \bar{P}\bar{v} + \bar{v}\bar{u}^2 + 0.5\bar{P}^2 + \bar{u}^2\bar{v}^2 + \bar{P}\bar{u}^2 + \bar{P}\bar{v}^2] \quad (A.7)$$

$$\rho_7 = \frac{\rho}{4}[-\bar{u}\bar{v}^2 + \bar{u}\bar{v} - \bar{P}\bar{u} - \bar{P}\bar{v} - \bar{v}\bar{u}^2 + 0.5\bar{P}^2 + \bar{u}^2\bar{v}^2 + \bar{P}\bar{u}^2 + \bar{P}\bar{v}^2] \quad (A.8)$$

$$\rho_8 = \frac{\rho}{4}[\bar{u}\bar{v}^2 - \bar{u}\bar{v} + \bar{P}\bar{u} - \bar{P}\bar{v} - \bar{v}\bar{u}^2 + 0.5\bar{P}^2 + \bar{u}^2\bar{v}^2 + \bar{P}\bar{u}^2 + \bar{P}\bar{v}^2] \quad (A.9)$$

$$\rho_9 = \frac{\rho}{24}[-2\bar{u} + \bar{u}^4 - \bar{P} - \bar{u}^2 + 6\bar{P}\bar{u}^2 + 1.5\bar{P}^2 + \overline{2u^3} + 6\bar{P}\bar{u}] \quad (A.10)$$

$$\rho_{10} = \frac{\rho}{24}[-2\bar{v} + \bar{v}^4 - \bar{P} - \bar{v}^2 + 6\bar{P}\bar{v}^2 + 1.5\bar{P}^2 + \overline{2v^3} + 6\bar{P}\bar{v}] \quad (A.11)$$

$$\rho_{11} = \frac{\rho}{24}[+2\bar{u} + \bar{u}^4 - \bar{P} - \bar{u}^2 + 6\bar{P}\bar{u}^2 + 1.5\bar{P}^2 - \overline{2u^3} - 6\bar{P}\bar{u}] \quad (A.12)$$

$$\rho_{12} = \frac{\rho}{24}[+2\bar{v} + \bar{v}^4 - \bar{P} - \bar{v}^2 + 6\bar{P}\bar{v}^2 + 1.5\bar{P}^2 - \overline{2v^3} - 6\bar{P}\bar{v}] \quad (A.13)$$